



# Effects of Loading Rate Range on Mechanical and Microstructural Properties of Dynamically Compacted Iron Powder

N. Namazi<sup>1</sup> · M. Alitavoli<sup>1</sup> · H. Babaei<sup>1</sup>

Received: 6 January 2020 / Accepted: 17 February 2020 / Published online: 27 February 2020  
© The Korean Institute of Metals and Materials 2020

## Abstract

In this paper, an attempt was made to investigate the effects of dynamic loading rate on the properties of iron powder with a focus on the microstructural characteristics of the compacted material. Dynamic compaction tests were performed using an instrumented die equipped with a load cell under the low loading rate ranging from 20 to 44 kN/ms in a drop hammer and the high loading rate ranging from 308 to 665 kN/ms in a one-stage light gas gun. Optical and scanning electron microscopes, diametric compression test, and Vickers hardness measurement were used to investigate microstructural and mechanical properties of the green compacts. The obtained results show that the range of loading rate completely changes the behavior of the powder by changing the number and velocity of the propagating stress waves. Comparison of the properties of specimens with equivalent density compacted under two ranges of loading rates indicates that the high range significantly increases the strength and hardness, distributes stress and porosity more uniformly, and reduces initiation and growth of inter-particle cracks as well as the compaction force required to achieve a specific density.

**Keywords** Loading rate · Dynamic compaction · Microstructural analysis · Mechanical properties · Iron powder

## 1 Introduction

Powder metallurgy (PM) has always been considered as a promising manufacturing method in many industrial applications due to excellent advantages of the process like a low waste of raw materials, near-net-shape components with complex geometries, high production rate, and controlling the degree of porosity. The conventional PM process includes mixing powder particles with additives (binder and lubricant), quasi-static die compaction of powder particles and subsequent sintering treatment to enhance the integrity and strength of the green compacts. Despite these advantages, PM faces limitations in compaction or sintering stages for some particular applications. For example, high levels of force must be applied for compaction of powders with high degrees of hardness [1]. Also, heating the compacts with high melting point needs high levels of temperature to complete the inter-particle melting process during the sintering stage [2]. In recent years, many efforts have been made to

overcome these limitations and modify the conventional PM process. Dynamic compaction (DC) is one of these modifications that has attracted considerable attention among PM researchers. DC is a high rate forming technique that leads to large localized plastic deformations and bonding between particles due to stress wave propagation [3]. DC has been implemented in many studies using different methods such as high-velocity impact of an impactor in a dynamic loading set-up like gas gun [4], drop hammer [5], hydraulic gun [6], direct or indirect explosion of charge [7, 8], and sudden discharge of electric current into the powder column placed inside an electrically non-conductive container [9]. Most of these studies have focused on the potential of this method for compacting different types of powdered materials like ceramics [10], polymers [11] and composites [12] as well as investigating different properties of the obtained compacts. The results show that DC leads to final products with less porosity, more uniform density and better mechanical properties in comparison with those obtained by the conventional PM process [13].

Properties investigation of the components obtained from iron-based powders is one of the most important research topics in the field of PM because of the broad application of these parts in different industries such as aerospace,

✉ M. Alitavoli  
tavoli@guilan.ac.ir

<sup>1</sup> Department of Mechanical Engineering, University of Guilan, P.O. Box 3756-41635, Rasht, Iran

automotive, electronics, petroleum, and agriculture. In recent years, different aspects of compaction of iron-based powders under dynamic loading have been studied in some researches. For example, Sethi [14] showed that the energy required to achieve a specific density under DC increases with the particle size as a result of more uniform distribution of energy for particles of smaller size. Furthermore, Sethi et al. [15] studied the effects of compaction pressure on dynamically pressed iron-based powder. Their results showed that at least 1.1 GPa pressure is required to produce components with full density in DC. Wang et al. [16] investigated the effect of different compaction profiles in DC of iron powder and concluded that applying a pre-compaction stage increases the mechanical properties of the compacted material. Zhang et al. [17] studied the effect of temperature during DC of iron-based alloy powder. They showed that increasing the temperature of the die during DC leads to an increase in the density, tensile strength, and hardness of the compacts.

Review of the literature related to DC of metal powders shows conflicting reports about the effects of the method on the microstructure of compacts. Some studies have reported desirable effects of DC like refined microstructure and good metallurgical bonds between particles [18], while some others have claimed that the process leads to microstructural defects like micro-cracks [19]. This contradiction may be due to the limited applied range of loading rate that has been considered as the evaluation criterion for microstructural effects of DC method. The main aim of this research is to investigate mechanical and particularly microstructural effects of dynamic loading rate. To provide a wide range of loading rates, iron powder has been subjected to impact loading using a drop hammer (low loading rate ranging from 20 to 44 kN/ms) and a gas gun (high loading rates ranging from 308 to 665 kN/ms) set-ups. Density, strength, and hardness of the obtained compacts have been evaluated to study the effects of dynamic loading rate on the mechanical properties. Also, the microstructure of the specimens was examined using Scanning Electron Microscope (SEM) and Light Optical Microscope (LOM) images to evaluate microstructural effects of dynamic loading rates.

## 2 Experimental Procedure

### 2.1 Raw Materials

Water-atomized iron powder (Qazvin Powder Metallurgy Co., Iran) was used in experiments of the present study because of its great application potential. Table 1 and Fig. 1 present the chemical composition and SEM image of the as-received powder. As shown in Fig. 1, powder particles

**Table 1** Percentage composition of the as-received iron powder (in wt%)

Element	Ni	Mo	Mn	O	Fe
Percentage	1.9	0.55	0.2	0.15	Balance

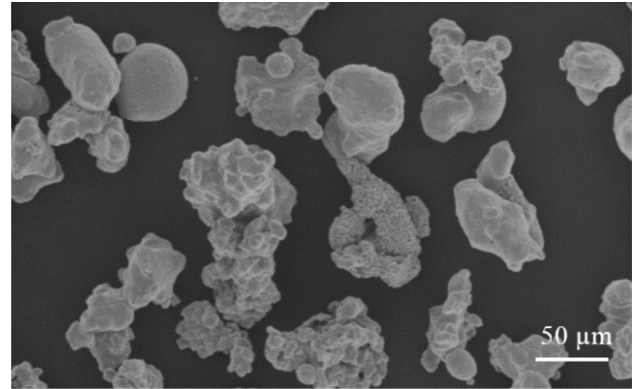


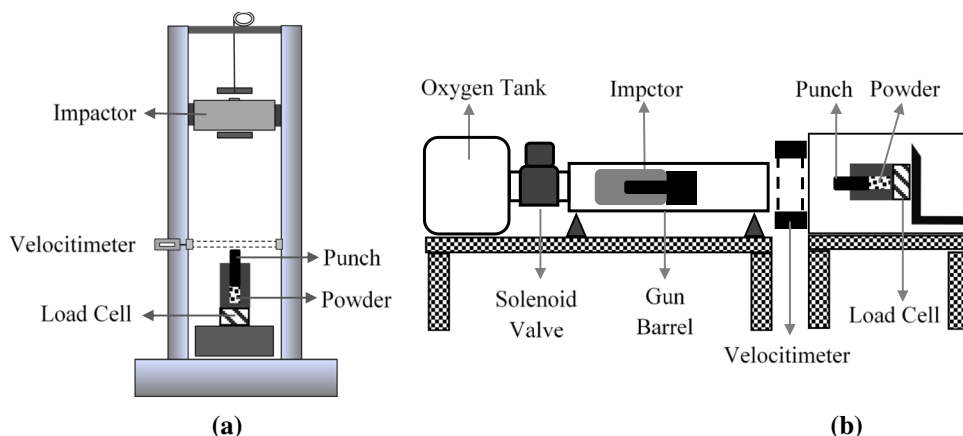
**Fig. 1** SEM image of the as-received iron powder

have irregular morphology with a size distribution of less than 65  $\mu\text{m}$ .

### 2.2 Instruments

To provide a wide range of dynamic loading rates, DC experiments were performed using two set-ups including a drop hammer (low loading rate ranges from 20 to 44 kN/ms) and a single-stage light gas gun (high loading rate ranges from 308 to 665 kN/ms) as shown in Fig. 2. In both cases, kinetic energy is transmitted to the powder due to the collision of an impactor with a punch. This densifies the powder and converts it from a loosely packed bed to a rigid part. The impactor velocity at the collision moment (compaction velocity) was measured with a laser velocitimeter. In each test, having the compaction velocity ( $v$ ) and mass of the impactor ( $m$ ), the compaction energy delivered to the powder can be calculated ( $E = \frac{1}{2}mv^2$ ). Different compaction velocities were obtained by releasing the impactor weighing 55 kg from different heights up to 6 m in the drop hammer as well as firing the impactor weighing 0.55 kg under different tank pressures up to 100 bar through a gun barrel of length 6 m in the gas gun. To reduce friction and improve the acceleration of the impactor in the gun barrel, the impactor was placed into a polyethylene cover in the gas gun tests (for more details about the drop hammer and gas gun set-ups used in experiments, one can see [20] and [21], respectively). Both the die (inner and outer diameter of 20 mm and 60 mm, respectively) and the punch (diameter of 19.5 mm) were made of 1.6582 steel hardened to

**Fig. 2** Schematic view of DC experimental assemblies: **a** drop hammer (for the low range of loading rates), **b** gas gun (for the high range loading rates)



40 HRC by heat treatment to resist against impact loading. Compaction force transmitted to the powder was measured by a strain gauge load cell positioned at the bottom of the die. In each test, variations of voltage versus time measured by strain gauges were amplified using a voltage amplifier and then recorded in a digital storage oscilloscope. Afterward, A scale factor of  $1 \text{ mV} = 63.183 \text{ N}$  was used to convert voltage waveforms to force pulses.

**2.3 Description of Experiments**

In each test, 30 g of the as-received iron powder was poured into the un-lubricated die equipped with the load cell at the bottom. Then, the assembly was subjected under impact loading in the drop hammer/gas gun and the obtained compact was ejected from the die using a 10-ton hydraulic press. Figure 3 shows the load cell assembly used in the gas gun experiments and a typical specimen obtained from DC test. Density, strength, hardness, and microstructure are the most important quality characteristics that should be considered in PM components. By measuring the mass and volume of the obtained

compacts, apparent density can be calculated. The ratio of this value to the theoretical density of iron powder ( $\rho_t = 7.87 \text{ gr/cm}^3$ ) gives a parameter called relative density that was used to compare the density of the compacts in this study. Also, the diametric compression test was used to evaluate compacts strength. To perform this test, the cylindrical specimen was subjected under compressive load between two flat plates in a universal testing machine (STM-250, Santam Co, Iran). The loading rate was set to be 0.5 mm/min and the corresponding force–displacement curve was recorded as demonstrated in Fig. 4. One can see that compressive force increases to a maximum value ( $F_{\text{max}}$ ) that corresponds to failure (initiation of the central crack) of the specimen and then drops rapidly. Then, the indirect tensile strength of the compact ( $\sigma_t$ ) was determined from the following expression [22]:

$$\sigma_t = \frac{2F_{\text{max}}}{\pi Dh_f} \tag{1}$$

where  $D$  and  $h_f$  are the diameter and height of the compact, respectively. This parameter was used to compare

**Fig. 3** **a** Load cell and die assembly in the gas-gun experiments, **b** a typical specimen obtained from DC test

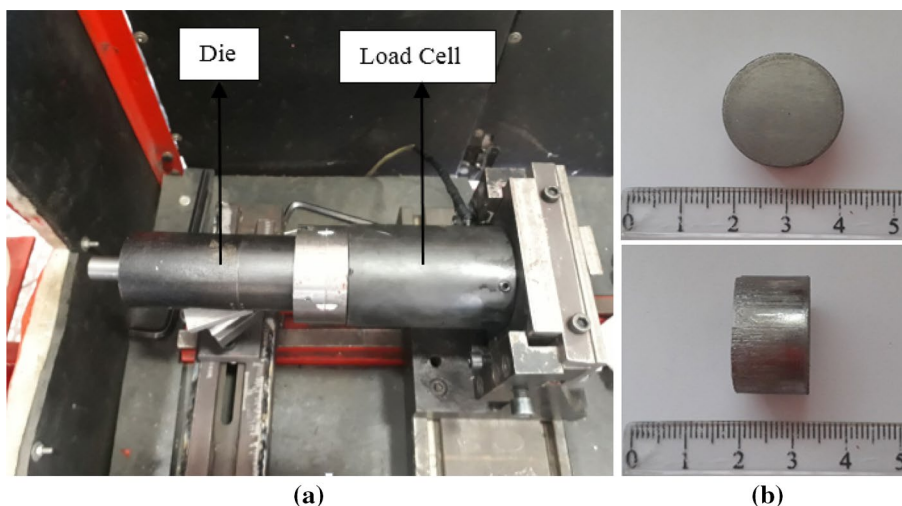


**Fig. 4** Diametric compression test: **a** specimen subjected to compressive load, **b** force–displacement curve obtained from the test

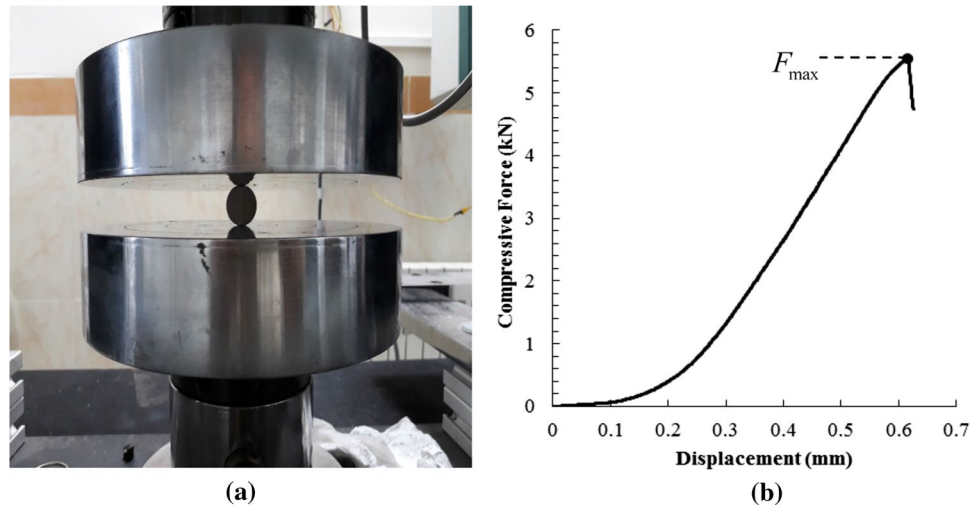


**Table 2** Test conditions and coding of samples

Test label	Set-up	$v$ (m/s)	$E$ (kJ)	$F_c$ (kN)	$t_c$ (ms)	$\dot{F}$ (kN/ms)
DH-1	Drop hammer	3.84	0.405	102.36	5.04	20.31
DH-2	Drop hammer	4.12	0.466	133.95	4.88	27.45
DH-3	Drop hammer	4.54	0.566	152.90	4.72	32.39
DH-4	Drop hammer	4.85	0.646	170.59	4.96	34.39
DH-5	Drop hammer	5.03	0.695	189.55	4.40	43.08
GG-1	Gas-Gun	58.24	0.932	96.04	0.312	307.82
GG-2	Gas-Gun	63.18	1.097	125.21	0.28	447.18
GG-3	Gas-Gun	67.51	1.253	140.27	0.296	473.89
GG-4	Gas-Gun	70.36	1.361	163.47	0.297	550.40
GG-5	Gas-Gun	74.48	1.525	187.02	0.281	665.55

the mechanical strength of the specimens. Vickers-scale calibrated hardness test was applied for hardness evaluation (Koop-UV1). In order to reach the hardness profile through the longitude axis, the hardness test was performed applying 1 kg force (HV1) on at least 10 surface points with the approximate distance of 1 mm from each other. Standard grinding and polishing procedure for preparation of metallographic specimens (ASTM E3-11) was used to examine the microstructure of compacts by LOM and SEM to find out how microstructural characteristics are affected by the range of loading rates. Table 2 presents different loading conditions for iron powder as well as coding of samples in DC tests. It is necessary to mention that, since the main aim of the present study is to focus on mechanical and particularly microstructural influences of dynamic loading rate, compaction velocities in the two set-ups were adjusted (trial and error) to result in specimens with nearly equal densities as much as possible (see Fig. 5).

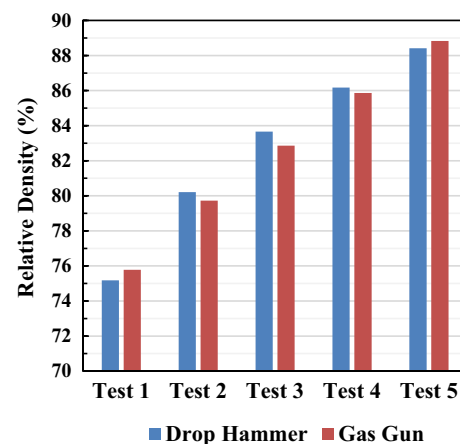
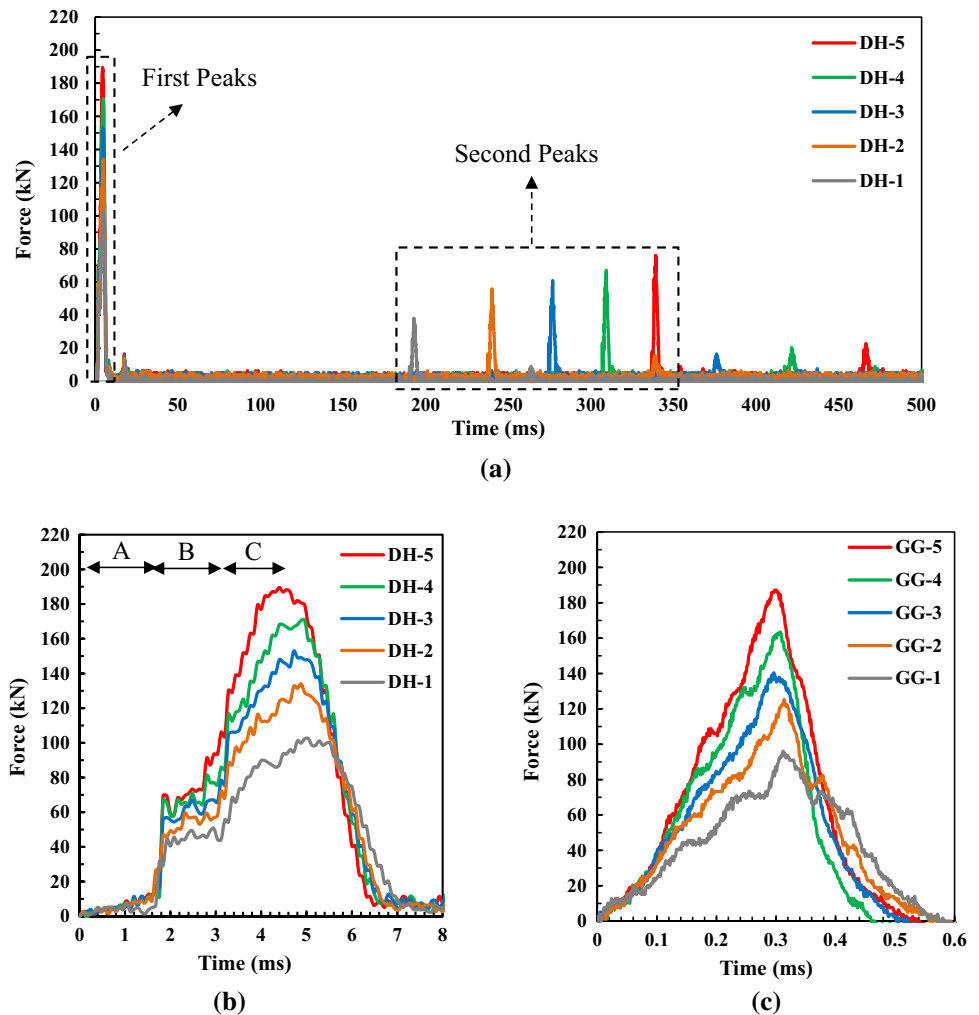


**Fig. 5** Corresponding relative density levels obtained by adjustment of compaction velocities in the two set-ups



**Fig. 6** Force-time response of iron powder during DC tests: **a** complete curves in drop hammer tests, **b** amplification of the first peaks in drop hammer tests, **c** gas-gun tests



### 3 Results and Discussion

Figure 6 illustrates force waveforms measured in the drop hammer (low loading rate) and gas gun (high loading rate) tests. In the case of drop hammer, a large amount of kinetic energy of the impactor is transmitted to the powder through the punch during the initial collision (first peaks) and the rest part causes the impactor to rebound and recollide with the punch (second peaks). Increasing compaction velocity leads to an increase in kinetic energy (i.e., more upward movement of the impactor) and delays the second peaks (see Fig. 6a). Figures 6b, c demonstrate amplification of the first peaks in the drop hammer and the force waveforms of gas gun tests, respectively. For all curves, dynamic force first increases up to a maximum point in the compaction (loading) process and then decreases rapidly during the de-compaction stage (unloading). The value of force and time at this maximum point is considered as the compaction force ( $F_c$ ) and compaction time ( $t_c$ ), respectively. In each test, the dynamic

loading rate can be obtained as the ratio of these two values ( $\dot{F} = \frac{F_c}{t_c}$ ). As can be noted in Fig. 6b, DC of iron powder in the low range of loading rates is a step-by-step process including three distinct stages (A–C) that can be separated from each other by two abrupt jumps in force value, whereas dynamic force has a monotonic pulsed waveform in the high range of loading rates (Fig. 6c) and no distinct stages can be distinguished. This difference can affect the stress distribution between the powder particles as well as energy dissipation during compaction. Stages A, B, and C can be considered in accordance with the three stages of particles deformation under quasi-static compaction (particle re-arrangement, elastic–plastic deformation, and cold working) that have been reported in many PM studies [23].

Simultaneous with the punch movement due to collision of the impactor, the material is subjected to uniaxial strain and incident stress waves, originated from the powder-punch interface, propagate within the powder and reflect successively from powder-die interfaces. In both ranges, dynamic

force in the compaction and de-compaction stages consists of tiny saw-tooth-like oscillations correspond to the interference of the incident and reflected stress waves within the powder. The number and actuation time are two significant characteristics of these successive waves that control the process. The former increases and the latter decreases in DC under the gas gun loading comparing to the drop hammer.

Propagation of incident stress waves within the powder increases force value (up to  $F_c$ ) leading to particles compression until release waves from the back surface of the punch arrive and un-load the post-compacted powder. For all curves in Fig. 6, compaction stage (i.e., propagation of plastic incident waves within the un-compacted powder) takes place in a longer time than the de-compaction phase that involves propagation of elastic waves with higher velocity in a post-compacted material. Since stress propagates within the powder through the interactions of particles in DC process, particles velocity that is determined by the propagation velocity of stress waves is a substantial parameter in powder behavior during the compaction and de-compaction stages. Comparing the average value of compaction time for two cases of experiments in Table 2 (4.8 ms for the drop hammer and 0.28 ms for the gas gun) indicates that stress

waves propagate with extremely higher velocity during the compaction process in the high range of loading rates. In both ranges, it is evident that as the compaction velocity rises, compaction force as well as propagation velocity of stress waves increase considerably as a result of increasing the amount of delivered kinetic energy (see Fig. 6b, c).

Figure 7 shows different microstructural events occur during DC under the low range of loading rates. At stage A, a low degree of acceleration is provided by low-amplitude stress waves for particles. Therefore, they can only move with low velocity and fill large pores during densification (Fig. 7a). When this stage completes, particles are located near each other in a tightly packed state having contacts with neighbors, so further densification can only occur by imposing plastic deformations. All metallic powders have an adherent surface layer of oxide that prevents metal–metal contacts and formation of proper inter-particle bonding. Characteristics of this layer play a significant role in the properties of final compacts [9].

Stage B begins with a jump in force value that creates high degrees of normal and shear stresses at small regions of contact between particles. As a result, breakage of the oxide layer and formation of metal–metal contacts occur that are

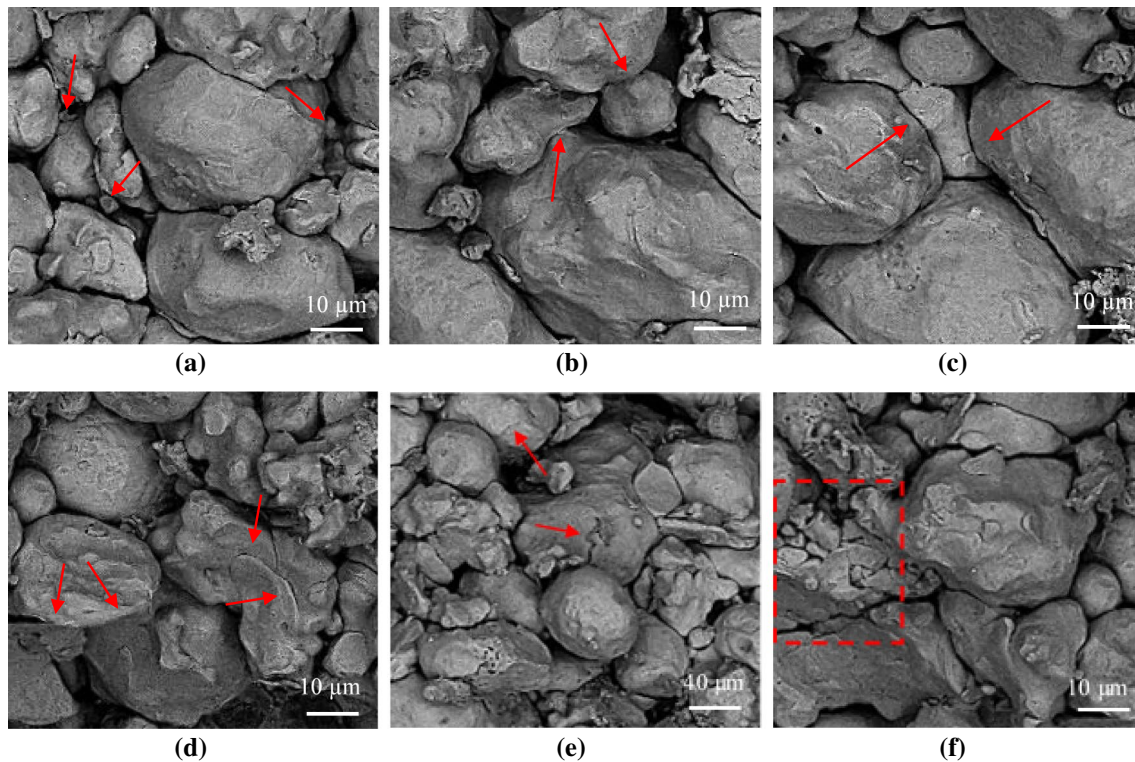


**Fig. 7** SEM images showing microstructural events in DC under the low range of loading rates: **a** porosity reduction due to filling large pores by small particles in stage A (DH-1), **b** plastic deformation at contact points leading to formation of solid bridges (DH-3), **c** plastic deformation at interfacial surfaces leading to formation of cold weld-

ing (DH-3), **d** plastic flow along with temperature rise at boundaries leading to thermal softening and subsequent frictional welding (DH-5), **e** initiation and growth of trans-particle cracks in large particles due to normal stress exerted from adjacent particles (DH-5), **f** particles fragmentation (DH-5)

necessary for inter-particle bonding. Increasing stress value continues until yielding the material around the contact region occurs that leads to localized plastic flow and formation of solid bridges (i.e., metallurgical bonding at contact points) between particles (Fig. 7b). The number of inter-particle bonds depends on the contact points that are provided for accelerated particles at the end of stage A. In some cases, a small particle, having more contact points, places between two or more particles with larger size which creates a multi-particle bond. Further increase in stress beyond the yield strength of the material enlarges particle–particle interfaces by imposing more plastic flow and deformation at interfacial surfaces. This leads to a decrease in the volume of pores as well as the formation of cold welding (two oxide-free metallic surfaces are brought into contact by inter-particle loads) between particles (Fig. 7c).

Also, extension of contact surfaces causes a temperature rise at the outer layers of particles due to interfacial friction. The heat generated at the boundary regions is conducted within the powder and causes the thermal softening phenomenon to occur. Thermal softening, in turn, contributes to intense localized shearing at boundaries and subsequent frictional welding between particles (Fig. 7d). Since no case of localized melting was observed in the microstructure of samples, it seems that temperature rise is not enough to melt the surface layer of iron powder particles compacted with the drop hammer. After force jump, stage B is followed by slightly increasing force value in a relatively long time interval (e.g., from 1.92 ms to 3.28 ms for DH-5). This step corresponds to the dissipation of energy through the extension of plastic flow to the inner layers of particles that deforms the shape of powder particles thoroughly.

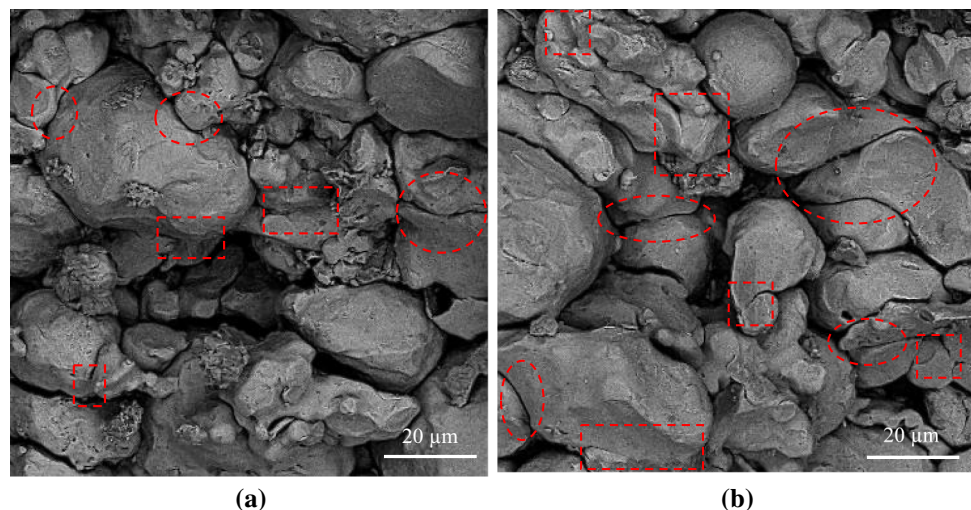
At the beginning of stage C, particles resist against further plastic deformation because hardening occurs in the following of compaction. As a result, the force curve experiences another jump to overcome the hardening of individual

particles. During this step, larger hardened particles, having less interfacial surface, may experience high degrees of normal stress from neighbors leading to nucleation and growth of trans-particle cracks (Fig. 7e). Also, a high amplitude force spike exerted on hardened particles may lead to fragmentation and grain size reduction (Fig. 7f). When this process completes, powder particles cannot be deformed individually and turn into a bulk material. Dynamic load again increases slightly and the bulk material is subjected to homogenous compression. This stage has a significant effect on the microstructural properties of the final compact because the work done by compaction force is stored within the material in the form of strain energy during bulk compression. This stored energy is the major factor leading to microstructural defects and residual stress during the decompaction phase [3].

In DC under the high range of loading rates, stress waves propagate within the powder with much more number and much higher velocity in comparison with the low range. Passage of high amplitude stress waves with short pulse time through the powder completely changes the powder response during compaction. Comparing force magnitude at the beginning of compaction stage in the gas gun (< 30 kN) and drop hammer (< 10 kN) reveals that particles movement occurs under a relatively higher load in the gas gun. The reason may be that in the high range of loading rates, a high enough level of force is needed to accelerate and high-velocity movement of particles in comparison with the low range that stress is only spent to aggregate them in a tight packing state and hence does not increase significantly.

Figure 8 shows the microstructure of specimens DH-4 and GG-4 with an equivalent level of density compacted using different set-ups. Comparison of Fig. 8a, b indicates that DC under the high range of loading rate increases the number and size of bonds in the form of cold welding and frictional welding. In DC under the high range of loading

**Fig. 8** SEM images showing the effects of the range of loading rate on the inter-particles bonding mechanisms in the form of cold welding (ellipses) and frictional welding (rectangles): **a** DH-4, **b** GG-4





rate, stress propagates within the powder through high amplitude pulses of short duration. This delivers a large amount of energy over a short period to powder particles causing a sudden increase in both stress and temperature at the outer layer. The average compaction time in the gas gun waveforms (0.29 ms) is such short that DC can be considered as an adiabatic process (i.e., there is not enough time for the generated heat and plastic flow to dissipate through penetration within the powder).

Furthermore, the movement and density of dislocations increase with loading rate and facilitate shear failure of the material in the high range [25]. Given these points, the number and area of inter-particles bonds are enhanced due to intensification of the stress and heat at the surface layer of powder particles. In addition to the formation of more successful bonds between particles, the high range of loading rate in the gas gun causes some unique phenomena, depicted in Fig. 9, to occur in the microstructure of the obtained compacts. Some particles are welded to each other through severe deformation at interfacial surfaces (Fig. 9a).

This may be contributed to high-velocity impact of particles during the compaction due to propagation of pulsed waveforms that leads to large plastic deformation at contact areas as well as metallurgical bonds. Close examination of the microstructure of GG-5 (obtained from maximum compaction velocity under the gas gun loading) reveals a thin layer of melting in the surface of some particles (Fig. 9b). This proves that temperature can increase up to the value that leads to melting the surface layer under the high range of loading rates. Figure 9c shows a powder particle with a very smaller grain size rather than the as-received state (Fig. 1) in the microstructure of sample GG-3. This may be due to the intense collision of particles as a result of high-velocity passage of stress waves that throws small crushed particles at the empty spaces between the larger ones. Also, intense localized shearing and thermal softening (resulted from adiabatic temperature rise) may cause extreme distortion at the boundaries of the impacted particles leading to the formation of material jetting phenomenon during the process, similar to that observed in explosive welding [24].

**Fig. 9** SEM image showing microstructural events in the specimens compacted using the gas gun: **a** sever interfacial plastic deformation and metallurgical bonding due to high velocity impact of particles (rectangle), **b** melting of surface layer due to adiabatic temperature rise (ellipse), **c** trapping of small particles between larger ones, **d** formation of interfacial material jets

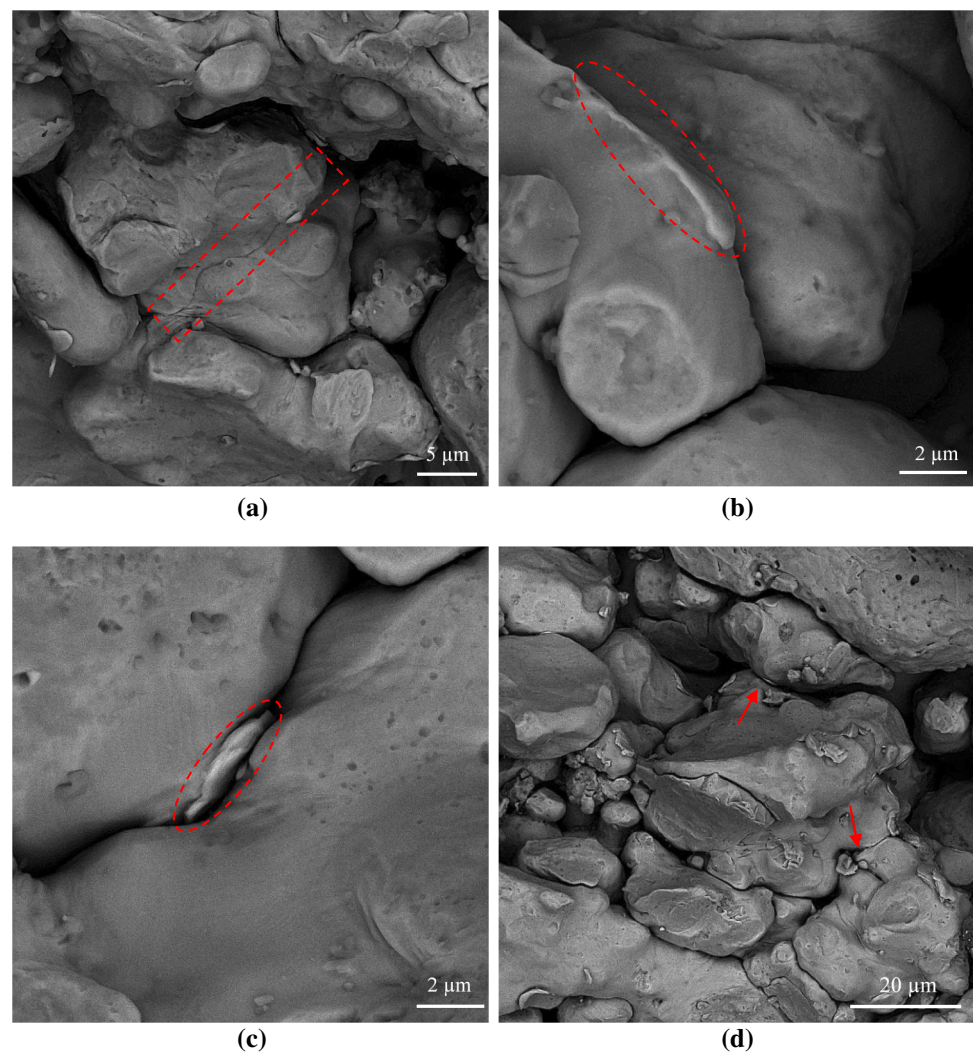
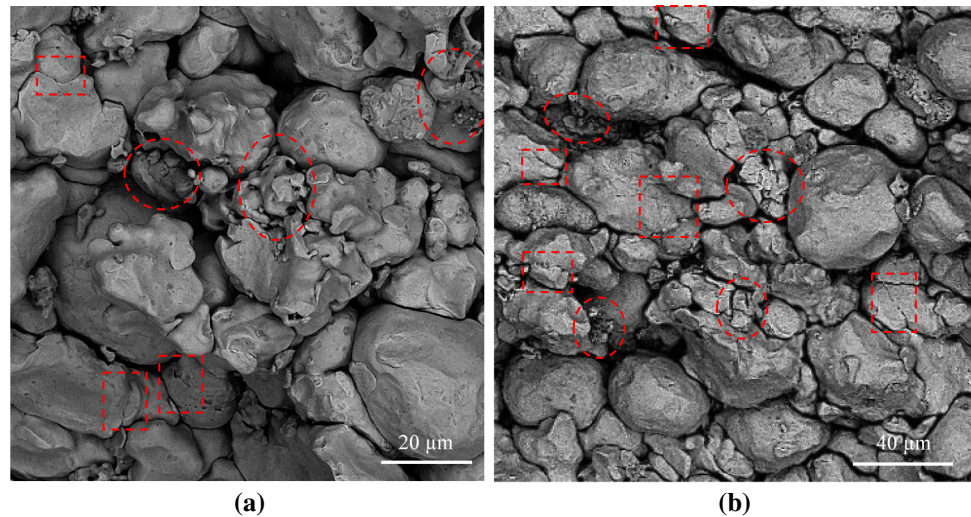


**Fig. 10** SEM image showing fragmented (ellipses) and cracked (rectangles) particles in the microstructure of specimens compacted under the low and high ranges of loading rates: **a** DH-3, **b** GG-3



These interfacial jets may be squirted into pores and causes inter-particle bonding (Fig. 9d).

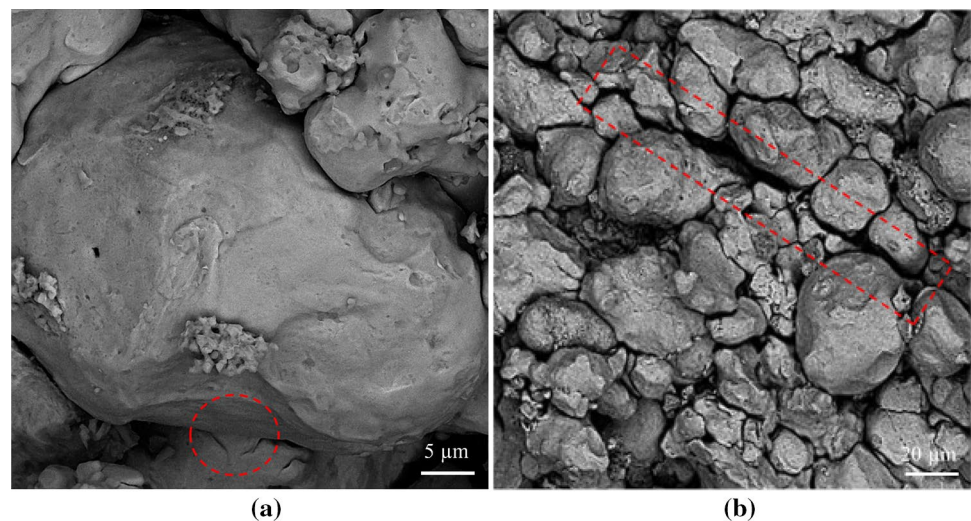
Figure 10 compares the microstructures of specimens DH-3 and GG-3 with an equivalent level of density. As indicated, there are more fragmented and cracked particles in the microstructure of sample GG-3 than DH-3. This may be due to that particles experience a higher degree of strain hardening under the high range of loading rates leading to a reduction in ductility of powder particles. Increment of the density of dislocations as well as confinement of energy dissipation to the outer surfaces accelerate fracture mechanism and subsequent grain-refinement process in the high range.

In DC under both ranges of loading rate, propagation of release waves during un-loading stage subject the generated inter-particle bonds to tensile stress. This causes the elastic recovery process to occur in which the pre-compacted rigid bulk tends to dimensional expansion after removing the punch. Compacts obtained under the low ranges include particles with weaker bonds and hence have less resistance to

de-bonding. Figure 11a shows a typical de-bonding between two particles in the microstructure of sample DH-3. Tensile stress exerted on inter-particle bonds increases with compaction force that may increase the number of de-bonded particles and subsequent inter-particle crack growth (see Fig. 11b). Figure 12 compares propagation and growth of inter-particle cracks in the specimens compacted under both ranges of loading rates. As can be seen, DC under the low range of loading rates increases the number and length of inter-particle cracks. Since the average time of de-compaction stage in the gas gun (0.24 ms) is much lower than the drop hammer (1.98 ms), there is more opportunity for cracks to initiate and growth during the elastic recovery process. Another factor may be associated with rebounds of the impactor that subject the compacted powder to successive impact loadings and cause inter-particle crack propagation.

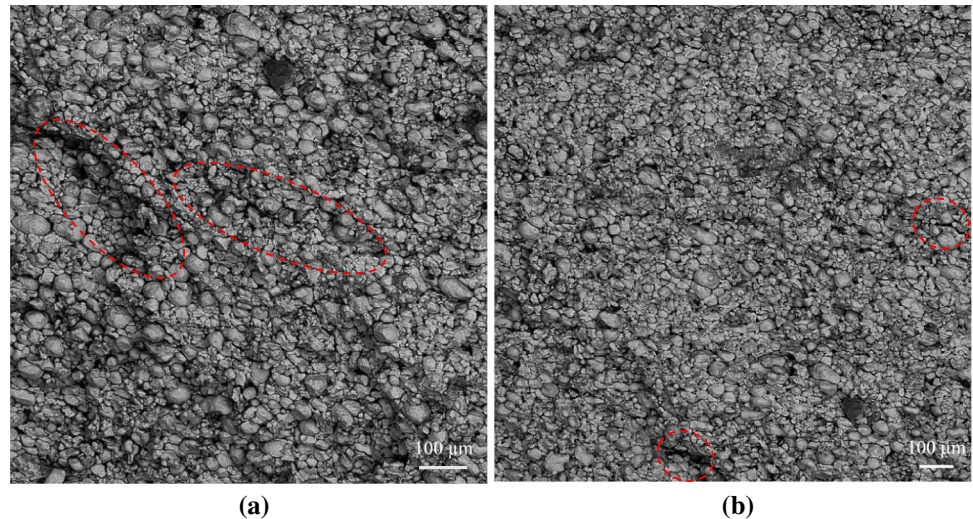
Figure 13 shows LOM image of the microstructure of two specimens with corresponding density compacted using two different set-ups. As can be seen, in both samples, the

**Fig. 11** Microstructural effects of the elastic recovery process during de-compaction stage: **a** a typical de-bonding between two particles in the microstructure of DH-3, **b** growth of inter-particle crack in the microstructure of DH-5

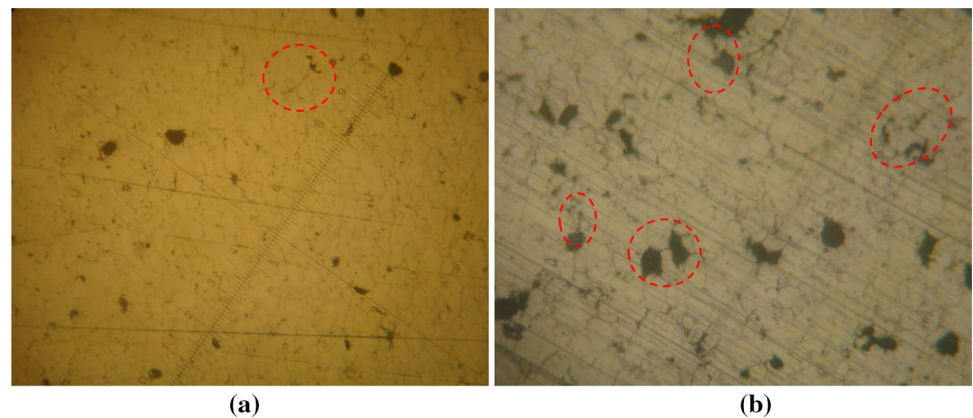




**Fig. 12** SEM image showing inter-particle crack propagation (ellipses) in the microstructure of the specimens compacted under the low and high ranges of loading rates: **a** DH-5, **b** GG-5



**Fig. 13** LOM image showing pore distribution and inter-particle crack propagation in the microstructure of specimens at 100× magnification: **a** GG-5, **b** DH-5



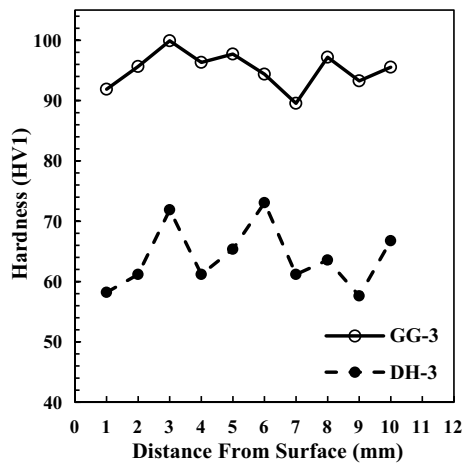
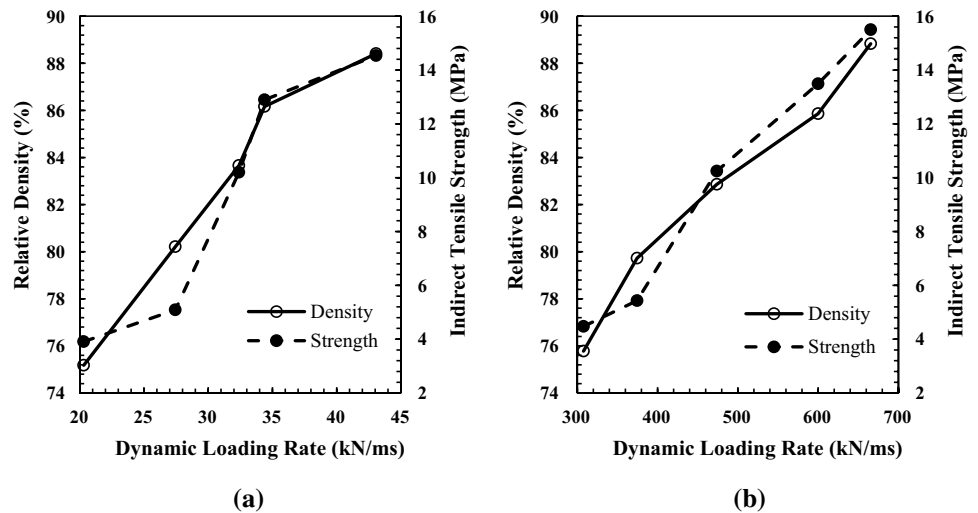
existing pores are the most potential places for the initiation and growth of inter-particle cracks. This is because the air is trapped in these locations and obstructs bonding between particles. Pores are distributed uniformly (both in size and location) in the microstructure of specimen GG-5 so that most initiated cracks stop growing and gradually diminish reaching the next pore location (see Fig. 13a), whilst many apparent pores in sample DH-5 are aggregated in specific regions (see Fig. 13b). Inhomogeneous distribution of pores under the low range of loading rate increases the number and growth length of inter-particle cracks in various directions (see Fig. 13b). As previously mentioned, the longer time of de-compaction stage under the low range of loading rates may be another reason that provides more opportunity for initiation and growth of cracks leading to an increase in the number and length of inter particle cracks. More successful metallurgical bonding and pore collapse resulted from intense plastic deformation along the boundary of particles are also evident in the microstructure of specimen GG-5.

Figure 14 shows variations of the relative density and indirect tensile strength with the loading rate in both ranges.

As shown in the figure, density and strength of the compacts increase with loading rate in both ranges due to the increase in the number and velocity of stress waves. Also, variations of hardness value along the specimens DH-5 and GG-5 are illustrated in Fig. 15. It can be seen that GG-5 (compacted under the high range of loading rate) have a higher degree and more uniform distribution of hardness than DH-5 (compacted under the low range of loading rate). This can be attributed to stronger bonds between particles and more uniform distribution of stress within the powder, respectively. Furthermore, adiabatic temperature rise confined at the outer surfaces causes powder particles to experience a higher degree of strain hardening by generating a rapid quenching state and may be considered as another explanation for increasing the hardness value of the sample GG-5.

Figure 16 compares indirect tensile strength as well as compaction force values for the specimens with corresponding levels of density (see Fig. 5). As illustrated, specimens compacted using the gas gun have higher mechanical strength (up to 14%) than those with equivalent density obtained under the drop hammer loading (Fig. 16a). This

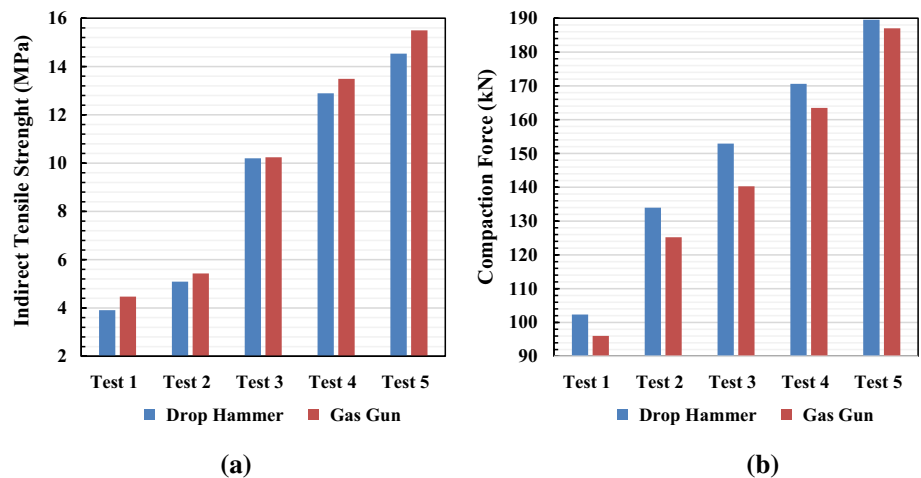
**Fig. 14** Variations of the relative density and indirect tensile strength for the compacts obtained from DC tests: **a** drop hammer, **b** gas gun



**Fig. 15** Hardness measurement along the height of specimens DH-5 and GG-5

shows that the high range of loading rates leads to stronger bonds between particles. Increasing the number and velocity of propagating stress waves causes uniform intensification of stress and temperature in the surface layer of particles due to adiabatic penetration and improves the strength of inter-particle bonds. Another observation in Fig. 16 is that DC under the high range of loading rate reduces the compaction force value required to obtain compacts with a certain level of density (see Fig. 16b). This may be attributed to a higher level of energy dissipation during DC process. Compaction force is proportional to the kinetic energy transmitted to the powder bed during DC. Under the high range of loading rates, a major fraction of kinetic energy absorbed by powder particles is dissipated through high-velocity impact of particles, development of intensified plastic flow at particles boundary, pore collapse, adiabatic temperature rise, and surface heating as well as grain fragmentation and cracking of hardened particles. This leads to stronger bonds between particles, enhancement of mechanical strength and hardness

**Fig. 16** Comparison of the specimens with corresponding relative density levels compacted under two ranges of loading rate in the DC tests: **a** indirect tensile strength, **b** compaction force values



of the obtained compacts as well as more uniform distribution of mechanical and microstructural properties.

Simultaneous reduction of the compaction force and enhancement of the mechanical strength for the compacts with equivalent density may also be attributed to the size of particles. Under the high range of loading, fragmentation of particles due to intense collision (Fig. 9c) and strain hardening (Fig. 10b) aggregates a lot of fine particles in local areas. Fine particles provide more interfacial surfaces and thus generates more inter-particle bonds. Additionally, small interfaces between fine particles create stress concentration regions and reduce the force required to form interfacial bonds. Fine particles easily fill the pores between large particles and increase the density (Fig. 9c). This is while increasing the density at the interfaces including large particles requires sufficient force to cause plastic deformation at the surface layers.

## 4 Conclusion

DC of water-atomized iron powder was investigated under two cases including low range (20 to 44 kN/ms in the drop hammer) and high range (308 to 665 kN/ms in the gas gun) of loading rates. Relative density and indirect tensile strength obtained from the diametric compression test were determined to evaluate the density and strength of the compacts. Since investigation of microstructural effects of dynamic loading rate was the main aim of the present study, various SEM and LOM micrographs were provided from the cross-section of the specimens. From the results obtained for the specimens with nearly equal densities, the following conclusions can be drawn:

- 1- Iron powder behavior under the high range of loading rates completely differs from that of the low range. The number and velocity of the stress waves propagated within the powder are the main factors that control powder behavior during compaction and de-compaction stages in both ranges.
- 2- Under the low range of loading rate, powder undergoes three different levels of stress that result in non-uniform distribution of microstructural and mechanical properties. However, under the high range of loading rate, stress has a pulsed waveform leading to an increase in the number and size of inter-particle bonds.
- 3- Comparison of the mechanical and microstructural properties of the specimens, having the same level of density but compacted under different ranges of loading rates, indicates that the high range increases the strength (number and size of inter-particle bonds) and hardness, distributes porosity more uniformly, and reduces ini-

tiation and growth of inter-particle cracks as well as compaction force required to achieve a certain level of density.

**Acknowledgements** This research did not receive any specific grant from funding agencies in the public, commercial, or not-for-profit sectors.

## Compliance with Ethical Standards

**Conflict of interest** The authors declare that they have no conflict of interest.

## References

1. R.K. Rajput, *A Textbook of Manufacturing Technology: Manufacturing Processes* (New Delhi, Laxmi, 2007), pp. 219–232
2. R.M. German, J. Ma, X. Wang, E. Olevsky, *Powder Metall.* **49**(1), 19–27 (2006)
3. G. Sethi, N.S. Myers, R.M. German, *Int. Mater. Rev.* **53**(4), 219–234 (2008)
4. D.A. Fredenburg, N.N. Thadhani, T.J. Vogler, *Mater. Sci. Eng. A* **527**(15), 3349–3357 (2010)
5. H. Babaei, T.M. Mostofi, M. Alitavoli, N. Namazi, A. Rahmampoor, *Geomech. Eng.* **10**(1), 109–124 (2016)
6. H. Li, H. Yin, D.F. Khan, H. Cao, Z. Abideen, X. Qu, *Mater. Des.* **57**, 546–550 (2014)
7. A.R. Farinha, M.T. Vieira, R. Mendes, *Adv. Powder Technol.* **25**(5), 1469–1473 (2014)
8. M. Alitavoli, E. Khaleghi, H. Babaei, T. Mostofi, N. Namazi, *Proc. Inst. Mech. Eng. Part E J. Process Mech. Eng.* **233**(2), 195–201 (2019)
9. A. Darvizeh, M. Alitavoli, N. Namazi, An investigation into the parameters affecting the breakdown voltage and inter-particle bonding in the electrical discharge compaction of metal powders. *Adv. Powder Technol.* **29**(10), 2346–2355 (2018)
10. T.J. Vogler, M.Y. Lee, D.E. Grady, *Int. J. Solids Struct.* **44**(2), 636–658 (2007)
11. B. Azhdar, B. Stenberg, L. Kari, *Polym. Test.* **24**(7), 909–919 (2005)
12. A. Atrian, G.H. Majzoobi, M.H. Enayati, H. Bakhtiari, *Int. J. Miner. Metall. Mater.* **21**(3), 295–303 (2014)
13. X. Yang, *Aust. J. Mech. Eng.* **15**(3), 182–186 (2017)
14. G. Sethi, *Pressing to full density: fundamental limitations and capabilities of high density powder metallurgy*, M.S. Thesis, The Pennsylvania State University, 2004
15. G. Sethi, E. Hauck, R.M. German, *Mater. Sci. Technol.* **22**(8), 955–959 (2006)
16. J.Z. Wang, H.Q. Yin, X.H. Qu, J.L. Johnson, *Powder Technol.* **195**(3), 184–189 (2009)
17. H. Zhang, L. Zhang, G. Dong, Z. Liu, M. Qin, X. Qu, *Powder Metall.* **59**(2), 100–106 (2016)
18. V.D. Linse, in *Innovations in Materials Processing*, ed. by G. Bruggeman, V. Weiss (Springer, Boston, 1985), p. 381
19. W.H. Gourdin, Local microstructural modification in dynamically consolidated metal powders. *Metall. Trans. A* **15**(9), 1653–1664 (1984)
20. A. Darvizeh, A. Meshkinzar, M. Alitavoli, R. Rajabiehfard, *Thin-Walled Struct.* **110**, 97–105 (2017)
21. R. Rajabiehfard, A. Darvizeh, M. Darvizeh, R. Ansari, M. Alitavoli, H. Sadeghi, *Thin-Walled Struct.* **107**, 315–326 (2016)

22. M. Çelik, *Pharmaceutical Powder Compaction Technology*, 2nd edn. (CRC Press, London, 2011), pp. 66–68
23. I. Cristofolini, G. Pederzini, A. Rambelli, A. Molinari, *Powder Metall.* **59**(1), 73–84 (2016)
24. A.M. Birt, V.K. Champagne, R.D. Sisson, D. Apelian, *Adv. Powder Technol.* **26**(5), 1335–1347 (2015)
25. K. Qin, L.M. Yang, S. Hu, in *Dynamic Behavior of Materials. Volume 1: Proceedings of the 2013 Annual Conference on*

*Experimental and Applied Mechanics*, ed. by B. Song, D. Casem, J. Kimberley (Springer, New York, 2013), p. 21

**Publisher's Note** Springer Nature remains neutral with regard to jurisdictional claims in published maps and institutional affiliations.